CHALMERS
UNIVERSITY OF TECHNOLOGY

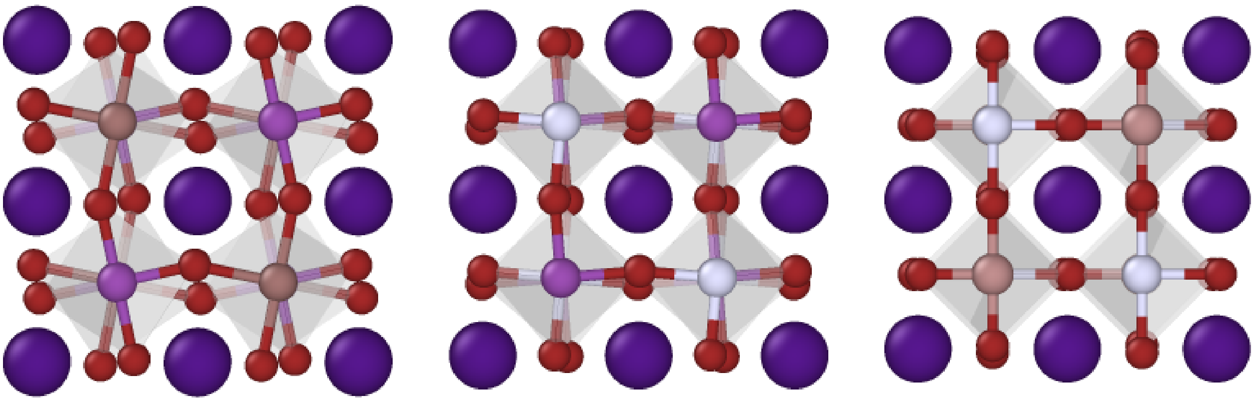

Towards More Efficient Solar Cells: the Effect of Dynamical Disorder on the Electronic Structure of Halide Double Perovskites

A Computational Study Examining the Effect of Lone-pair Electrons on the Octahedral Tilting and the Band Gap in Halide Double Perovskites

Master’s thesis in Engineering physics

Madeleine Karlsson

DEPARTMENT OF PHYSICS
CHALMERS UNIVERSITY OF TECHNOLOGY
Gothenburg, Sweden 2022
www.chalmers.se

Master's thesis 2022

Towards more efficient solar cells: the effect of dynamical disorder on the electronic structure of double halide perovskites

A computational study examining the effect of lone-pair electrons on the octahedral tilting and on the band gap in halide double perovskites

Madeleine Karlsson

Department of Physics
Condensed Matter and Materials Theory
Chalmers University of Technology
Gothenburg, Sweden 2022

A computational study examining the effect of lone-pair electrons on the octahedral tilting and on the band gap in halide double perovskites
MADELEINE KARLSSON

Supervisor: Julia Wiktor, Condensed Matter and Materials Theory
Examiner: Julia Wiktor, Condensed Matter and Materials Theory

Master's Thesis 2022
Department of Physics
Condensed Matter and Materials Theory
Chalmers University of Technology
SE-412 96 Gothenburg

Cover: Structures corresponding to double perovskites exhibiting different levels of octahedral tilting.

Typeset in LaTeX
Printed by Chalmers Reproservice
Gothenburg, Sweden 2022

A computational study examining the effect of lone-pair electrons on the octahedral tilting and on the band gap in halide double perovskites
MADELEINE KARLSSON
Department of Physics
Chalmers University of Technology

Abstract

Recently, simple perovskites have attracted great attention as energy-absorbing materials in solar cells. In computational and experimental studies they have shown several desirable properties but also challenges, such as instabilities and toxicity due to the presence of heavy metals, such as lead. As a solution to the problems connected to the simple perovskites, the double perovskites were suggested as suitable materials in the solar cells of tomorrow. In order to use double perovskites in an application they need to be thoroughly understood. Within this thesis the octahedral tilting and the band gap of double perovskites have been studied, which is a step towards finding a material that is stable and exhibit the optimal band gap for absorbing solar energy. It turns out that the octahedral tilting is not as prominent in all double perovskites as in the simple ones. The statement that the octahedral tilting is due to the presence of lone-pair electrons is considered and it agrees with the calculations - lone-pair electrons induce octahedral tilting. The effect of octahedral tilting on the band gap of the double perovskites is studied as well and it is concluded that the band gap increases with the tilting. So, as the global warming increases rapidly it is important to find green solutions and as solar cells produce renewable energy and are emission-free they are good candidates for further research and developement.

Keywords: perovskites, band gap, DFT, VASP, solar cells, phonons, lone-pair electrons, octahedral tilting

Acknowledgements

First of all, I would like to thank Julia Wiktor for being my supervisor and examiner. Thank you for all your time, encouragements and for your patience with all my questions. I am so grateful that you gave me the opportunity of working with this thesis, which has been so interesting and so much fun. I would also like to thank Paul Erhart and Erik Fransson for your brilliant inputs and suggestions.

Ambjörn, thank you for sharing an office with me during this spring and for patiently sharing your knowledge and Viktor, thank you for taking the time to take many cups of coffee with me.

Finally, I want to thank my Pontus and my family for your love and support during this thesis and also during the last five years. I could not have done it without you.

Madeleine Karlsson, Gothenburg, May 2022

Contents

List of Acronyms

Below is the list of acronyms that have been used throughout this thesis listed in alphabetical order:

CBM	Conduction Band Minimum
DFT	Density Functional Theory
PES	Potential Energy Surface
PV	Photovoltaic
VASP	Vienna Ab initio Simulation Package
VBM	Valence Band Maximum

List of Figures

List of Tables

1

Introduction

1.1 Background

One of the most urgent challenges we face today is the environmental issues with increasing temperature and chaotic weather conditions. As the climate crisis escalates and the demand for electricity grows it is crucial to continue develop techniques of producing green electricity. Today there are several choices of renewable energy sources, such as wind, hydro and solar energy and they each come with their own possibilities and challenges.

Focusing on solar energy, the first solar cell was created in 1883 and it was manufactured by coating selenium with a thin layer of gold. The inventor Charles Fritts stated that the solar cell produced a current *that is continuous, constant and of considerable force*. He had created a solar cell of an energy conversion rate, or efficiency, of 1 to 2 percent, compared to the modern solar cells of 15 to 20 percent. The energy conversion rate is the ratio between the power obtained from the solar cell and the incident solar power. In the 1950's, more than a hundred years later, the Bell Laboratories realized that semiconducting materials may be more efficient and produced the first silicon solar cell with 6 percent efficiency. However, the solar cells were still very costly and unavailable to the common man. The silicon solar cells have been developed since then and with their increasing efficiency it is today the most commonly used solar cell, despite the high cost [8]. Several attempts have been made to solve the challenges of the silicon solar cells, such as thin-film, organic or perovskite photovoltaics. Recently, much research has been made to understand the simple perovskites in order to use them in solar cell applications. Simple perovskites have been synthesized and have achieved an efficiency of 25 percent [9], but the stability of the material is relatively poor and the presence of lead results in the material being toxic. To face these challenges, the double perovskites were suggested as an alternative. They were shown to be more stable and can be manufactured without toxic constituents [5].

In order to use the double perovskites in solar cell applications, their structures and electronic properties need to be understood thoroughly. Apart from the material being stable and non-toxic it also needs to exhibit an appropriate band gap. The band gap is the key property to take into account when considering the energy conversion rate of a solar cell. There is an optimal value of the band gap of an energy-absorbing material given by the Shockley-Queisser limit which considers the excitation rate of the electrons and the recombination of the electrons and the holes [21]. In this thesis, the band gaps of different double perovskites are studied as a way of tuning them. It is a step towards understanding the double perovskites and eventually implementing them in commercial solar cells and then, hopefully, double perovskites can be a part of the solution to the environmental issues we face.

1.2 Objectives and limitations

This thesis is devoted to studying the effect of dynamical disorder on the electronic structure of the halide double perovskites. It is a computational study where density functional theory is used to calculate the structures and properties of various double perovskites. The aims of this thesis are to examine how the dynamics of the ions affect the properties, such as the band gap and the total energy of the perovskites, and to study how the inclusion of spin-orbit coupling affects the results. The results are mainly visualized as material specific phonon dispersion relations and potential energy surfaces and are also compared to the results of the simple perovskite case.

This thesis is limited to studying the double perovskites $Cs_2AgBiBr_6$, $Cs_2InBiBr_6$ and $Cs_2AgGaBr_6$ and the simple perovskite $CsPbBr_3$. The double perovskites exhibit several imaginary modes in the phonon dispersion relation which correspond to phonon instabilities in the materials. Due to the time limit of the thesis, only the first mode of the Γ-symmetry point is studied for the different materials. There are also several corrections and improvements available in order to ameliorate the results of the calculations. In this thesis, the spin-orbit coupling was included but the inclusion of semi-core electrons and hybrid functionals are left to be studied.

1.3 Thesis outline

The thesis is structured as follows. The second chapter covers the necessary theory in order to understand the methods used and the results. It gives a basic understanding of electronic structures, solar cells and perovskites. The third chapter includes approximations and theorems connected to the density functional theory. The computational details regarding the thesis are found in chapter four. The results and the associated discussions are presented in chapter five. Finally, chapter six contains a conclusion of the thesis and an outlook.

2

Theory

2.1 Electronic structure

The study of electronic structures and properties of atoms, molecules and condensed matter can be boiled down to the Schrödinger equation,

$$\begin{cases} H\psi(\mathbf{r}) = E\psi(\mathbf{r}) \\ \quad H = T + V. \end{cases} \tag{2.1}$$

From this equation the wavefunction, $\psi(\mathbf{r})$, and the discrete energy levels, E, of a quantum system can be calculated, given the Hamiltonian of the system, H, which includes the potential energy and the kinetic energy. A wavefunction is the description of the quantum state of a quantum system and it can be interpreted as a probability amplitude from which the probable whereabouts of the particles can be derived. An instructive example of a quantum system is the single particle of mass m in an one-dimensional infinite square well. This system yields the wavefunctions

$$\Psi_n(x) = \sqrt{\frac{2}{a}}\sin(\frac{n\pi}{a}x), \tag{2.2}$$

where a is the width of the well, and the following discrete energies,

$$E_n = \frac{n^2\pi^2\hbar^2}{2ma^2}, \ \ n = 1, 2, 3, ... \tag{2.3}$$

The number of energy levels of a particle is infinite [15]. The wavefunctions and energy levels described above are visualized in Figure 2.1.

An atom or a molecule are quantum systems, where each particle can be described by a wavefunction. The particle mainly considered in the scope of this thesis is the electron. The wavefunction of an electron orbiting an atom is called an atomic orbital and is described by different quantum numbers. There are, among others, the principal quantum number $n = 1, 2, 3, ...$ which corresponds to the distance of the electron from the nuclei and the angular quantum number $l =$ s,p,d,f,.. which is related to the shape and symmetry of the orbital. For larger atoms it is, in numerical calculations, common to only account for the valence electrons which are the ones contributing to the chemical properties of the atom [23].

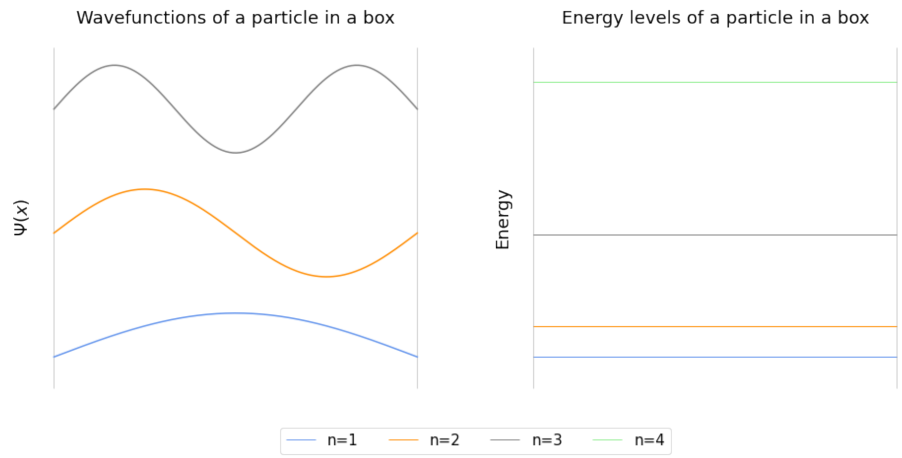

Figure 2.1: Wavefunctions and energy levels corresponding to a particle in a box. n is the principal quantum number.

2.2 Spin-orbit coupling

The spin-orbit coupling is a quantum effect which contributes to the total energy of a quantum system. According to the classical electromagnetic theory, a magnetic dipole moving in an electrostatic field is affected by a force proportional to the velocity of the dipole and the strength of the field. Viewing an electron orbiting an ion as a magnetic dipole, a coupling between the magnetic moment of the electron and the potential of the ion arises and this is the spin-orbit coupling. As an electron can exhibit either spin up or down, each electron orbit corresponds to two different energy values and this may cause fine structure in the spectra of the atoms.

With the help of electromagnetic theory, an expression of the energy contribution from the spin-orbit coupling with relativistic corrections can be obtained using

$$H_{SOC} = \frac{1}{2\mu^2 c^2 r} \frac{\mathrm{d}V(r)}{\mathrm{d}r} \vec{L} \cdot \vec{S}, \tag{2.4}$$

where μ is the reduced mass of the system, c is the speed of light, $V(r)$ is the potential energy at distance r, $\vec{L}$ is the angular momentum of the electron and $\vec{S}$ is the spin.

2.3 Lone-pair electrons

Atoms in matter interact with each other in different ways depending on their chemical properties. They form bonds between them which keep them in position relative to each other. There are, for example, the ionic bonds where positive and negative ions attract due to their charges and the covalent bonds where the atoms share valence electrons. These are important bonding types for the structures covered in this thesis.

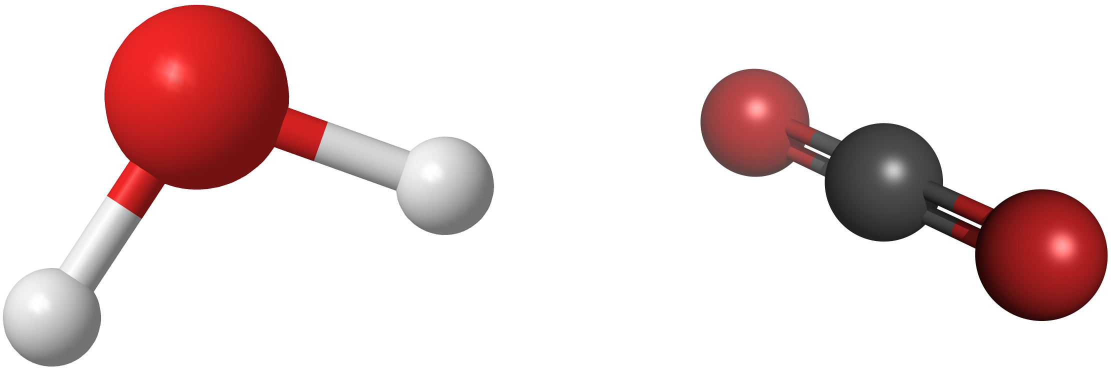

Figure 2.2: Illustrations of the water molecule and the carbon dioxide molecule. The water molecule is nonlinear with single covalent bonds and the carbon dioxide molecule is linear with double bonds.

When atoms form covalent bonds they share electrons in order to form a full outer shell. However, there may be electrons not participating in any covalent bonding which results in the forming of lone-pair electrons. Lone-pair electrons is a pair of electrons that is not shared with other atoms. These lone-pair electrons affect the structure and dynamics of the surrounding atoms in the system. A descriptive example of the effect of lone-pair electrons on a structure is the difference between a water molecule, H_2O, and a carbon dioxide molecule, CO_2. These two molecules are illustrated in Figure 2.2.

The water molecule consists of an oxygen atom, with six valence electrons, which is covalently bonded to two hydrogen atoms. This leaves the oxygen atom with two lone-pair electrons. The carbon dioxide molecule on the other hand contain one carbon atom and two oxygen atoms, which are covalently bonded as well. In this case the carbon atom's four valence electrons do not form any lone-pair electrons. Looking at the structures of the molecules in Figure 2.2 it is apparent that the carbon dioxide is a linear molecule where the bond angle is 180° and the water molecule is a non-linear molecule. This is a result of the high negative charge density of the lone-pair electrons connected to the oxygen atom in the water molecule, forcing the covalently bonded hydrogen atoms downwards while the carbon dioxide molecule remains linear due to the lack of lone-pair electrons of the carbon atom [1].

Lone pair electrons can, as mentioned earlier, affect the structure and dynamics of atoms and by extension also the properties of the material. The presence of lone-pair electrons may result in anharmonic dynamics and it is essential to understand the chemistry of the lone-pair electrons in order to grasp the full potential of a material.

2.4 Crystal and reciprocal lattices

The atoms in a solid material are placed in a crystal lattice, which, in theory, is constructed of infinitely many unit cells. This infinitely large, periodic lattice is a so-called *Bravais lattice* and it is defined by three basis vectors, $\mathbf{a}_{1,2,3}$. The different lattice sites of the crystals are given by linear combinations of the basis vectors,

$$\mathbf{R} = \sum_{i=1}^{3} n_i \mathbf{a}_i, \tag{2.5}$$

where n_i is an integer. The periodicity of the lattice may be, when considering the potential in the lattice, described by the following expression

$$V(\mathbf{r}) = V(\mathbf{r} + \mathbf{R}), \tag{2.6}$$

where $\mathbf{r}$ is the vector to any position inside the unit cell. The potential remains the same when adding a lattice vector $\mathbf{R}$ to the position vector $\mathbf{r}$. Of course, in reality the structure and periodicity of the lattice are not perfect; thermal vibrations and defects causes irregularities in the material.

In addition to the crystal lattice there is the reciprocal lattice which describes the Fourier transform of the crystal lattice. The reciprocal lattice represents the crystal lattice in momentum space, or $\mathbf{k}$-space, where the momentum is depicted by the wave vector $\mathbf{k} = \frac{2\pi}{\lambda}$. λ is the wavelength of the wave which is connected to the dynamics of the atoms in the real space. In order to describe this lattice, the reciprocal lattice vectors, $\mathbf{G}$, are defined as the vectors to all reciprocal lattice points. The reciprocal vectors may be viewed as wave vectors that yield plane waves and they are restrained by the following constraints, which corresponds to equation 2.6,

$$\begin{cases} e^{i\mathbf{G}\cdot\mathbf{r}} = e^{i\mathbf{G}\cdot(\mathbf{r}+\mathbf{R})} \\ \mathbf{R}\cdot\mathbf{G} = \quad 2\pi n. \end{cases} \tag{2.7}$$

n is also here an integer. From Equation 2.7 an important property may be derived. A larger distance, R_i, in the crystal lattice corresponds to a smaller distance in the reciprocal lattice, G_i, and vice versa. The index i represents a specific point in the crystal lattice and its corresponding point in the reciprocal lattice. The spatial periodicity of the Bravias lattices is easily described in momentum space and this is one of the great advantages of using the reciprocal lattice contrary to the regular arrangement of atoms.

Because of the periodicity of the reciprocal lattice it is an advantage to define the *Brillouin zone* which is the volume in the reciprocal space which is closer to the chosen origin than any of the other lattice points. All information about the periodic lattice is contained in this region and is then repeated infinitely many times as reciprocal lattice vectors are added to the wave vector [16].

2.5 Solar cells

2.5.1 Semiconductors

A semiconductor is a type of material which does not transport electricity very well but not extremely poorly either. A semiconductor has a band gap, the energy difference between the valence band and the conduction band, which allows for some of the electrons from the valence band to be excited to the conduction band through absorption of energy. This transition results in free electrons which can move in the material with small hindrance. The excited electrons which have transitioned to the conduction band leave behind holes in the valence band. The holes can be seen as positive charge carriers while the electrons in the conduction band act as negative charge carriers. These charge carriers are responsible for conducting the electrical current through the material. As can be derived from the following equation, called the Fermi-Dirac equation, a higher temperature increases the possibility of an electron in the valence band to transition to the conduction band which is an advantage in obtaining an electrical current. The Fermi-Dirac equation is written

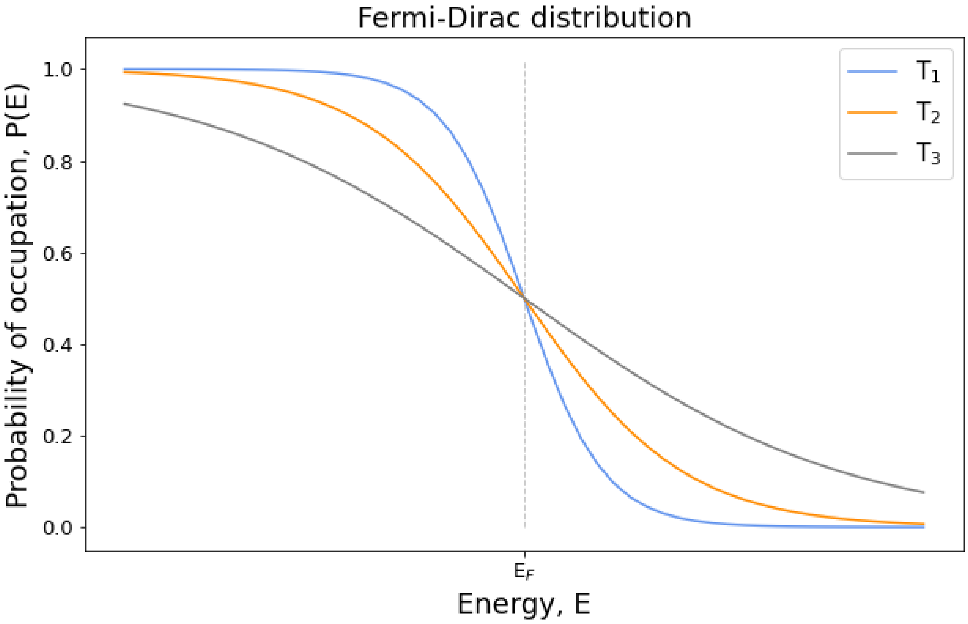

Figure 2.3: Visualization of the Fermi-Dirac distribution for different temperatures, $T_1<T_2<T_3$. E_F represents the Fermi energy.

$$p(E) = \frac{1}{e^{(E-E_F)/kT}+1}, \tag{2.8}$$

where k is Boltzmann's constant, T is the temperature and E_F is the Fermi level.

2.5.2 Principles of solar cells

The energy-absorbing materials in solar cells are semiconductors where the energy from the sun in the form of photons is absorbed by the electrons. This enables the electrons to transition from the valence band to the conduction band. As mentioned in section 2.5.1, the negative and positive charge carriers, which are formed through excitation of an electron, are responsible for conducting the electrical current through the material towards conducting metal contacts which lead the current further. On the journey of the electrons and the holes through the material there is a possibility of recombination of the two charge carriers which decreases the number of free electrons and thereby also the efficiency of the solar cell. Recombination of two charge carriers means that the free electron loses energy and falls back into the valence band where it again combines with the hole. Recombination can result in the release of a photon (radiative recombination), generation of heat in the material (non-radiative recombination) or the release of an Auger electron. The possibility of recombination increases with decreasing bandgap, which is why it would be inefficient to use a conductor, such as a metal, which has no bandgap as absorbing material in a solar cell. In a solar cell there is an ongoing battle between creation and recombination of the charge carriers. A smaller bandgap would increase the number of excited electrons and holes but this would also result in an increment of the number of recombinations of charge carriers. There is an optimal band gap which results in the highest possible electric current. This band gap occurs at the so called Shockley-Queisser limit [21] and is estimated to 1.3 eV [19].

In order to prevent recombination and thereby obtain a larger current it is necessary to seperate the different charge carriers. The solar cell therefore requires an asymmetry which drives the two different carriers to behave differently. Assuming a silicon solar cell, it relies on the asymmetry of homojunctions. A homojunction consists of two parts of the same material forming a junction. The two different parts are respectively p- and n-doped which, when the two parts are in contact, leads to diffusion of electrons from the n-doped to the p-doped side while the holes flow in the opposite direction. This creates a depletion region between the two semiconductors which contains no charges, but instead induces an electric field which opposes the diffusion mechanism. Since the electrons and the holes are affected by the electric field in opposite directions the charge carriers are separated. If instead a perovskite cell is considered, it adopts the properties of a heterojunction to seperate the charge carriers. A heterojunction consists of two semiconductors with different bandgaps. The different bandgaps will give rise to a discontinuity in the valence and conduction bands which causes one type of carrier to be blocked while the other can pass through. Based on these two ways of obtaining asymmetry in the material, the charge carriers are separated which reduces the possibility of recombination resulting in a higher efficiency of the solar cell [23].

2.6 Halide perovskites

2.6.1 Halide simple perovskites

Halide perovskites is a class of materials, some of which have properties that make them suitable for optoelectronic devices, as decribed in section 2.5. Several of the different materials in this class have therefore been studied extensively during the past years [5]. The simple halide perovskites can be seen as a subclass of the halide perovskite class and has the chemical formula ABX_3, where A is a monovalent cation, B is a divalent cation and X is a monovalent halide anion [23]. A cation is a positively charged ion in contrast to the anion which is negatively charged. The monovalent ions have one charge (positive or negative) while the divalent ion has two charges [22]. Halide, or halogenide, specifies that the anion is a halogen ion (Cl, F, Br etc). The halogen ions form octahedra with a divalent cation in the center of the octahedra and a monovalent cation between the octahedra. The structure of the simple halide perovskite is visualized to the left in Figure 2.4. In the figure, the blue ions are monovalent cations, the red ones are the halides and the grey represents the divalent cations. Generally, the atoms on the B and X site interact by mostly ionic bonds, but also covalent bonds. The A atom has no bonds to the nearby atoms, B and X [24]. Different types of simple halide perovskite have had a rapid development over the past years however it is not commercialized, mainly because of two crucial problems:

- poor structural stability when exposed to light, heat, humidity, electric fields, oxygen etc.
- the heavy metals, such as Pb, causes an intrinsic toxicity in the material [5].

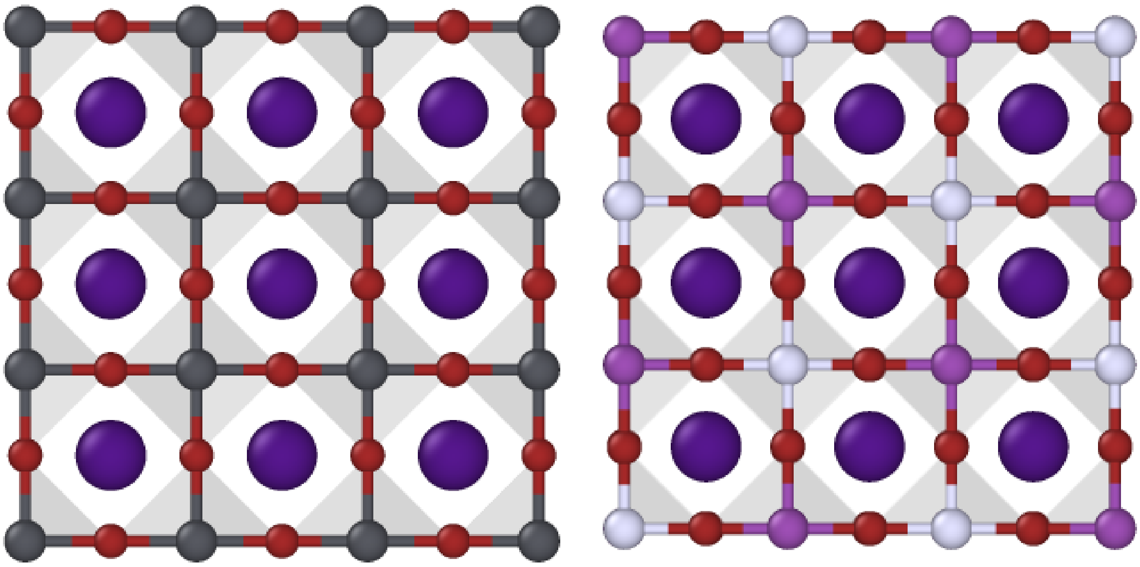

Figure 2.4: *Left*: Structure of the simple perovskite $CsPbB_3$ in the cubic phase. *Right*: Structure of the double perovskite $Cs_2AgBiBr_6$ in the cubic phase. Here, red is Br, blue is Cs, grey is Pb, purple is Bi and white is Ag. The grey areas represent octahedra.

2.6.2 Halide double perovskites

The halide double perovskites (HDP) were proposed by Volonakis et al [3] in 2016 as a possible solution to the problems for the simple perovskites which are listed above. They substituted the B^{2+} ion for a B^{+}/B^{3+} pair which results in HDP having the chemical formula $A_2B_2X_6$ or $A_2B^{+}/B^{3+}X_6$. Generally, the structure consists of alternating $B^{+}X_6$ and $B^{3+}X_6$ octahedra with the same cation inhabiting the A-site in the center of the cuboctahedral cavity. The monovalent A-site may be occupied by Cs^{+}, Rb^{+}, CH_6N^{+} or $C_4H_{12}N^{+}$. Examples of the B-site ions are Ag^{+}, Cu^{+}, Bi^{3+} and Sb^{3+} and the X-sites are occupied by a monovalent halide anion, such as Cl^{-},

Br^- or I^- [5]. The structure of a double perovskite in cubic phase is visualized to the right in Figure 2.4.

2.6.3 Harmonic instabilities

An important concept when dealing with halide perovskites is phonon instabilities. The atoms are not completely fixed at their equilibrium positions in real-life applications and the motions of the atoms result in different instabilities and distortions in the material. The instability which will mainly be considered within this thesis is the tilting of the octahedra consituted of the B-site ions. The octahedral tilting is temperature dependent. When the ions are exposed to a high temperature the ions adopt an high-symmetry cubic structure, when taking the average of the ions' positions during a period of time. On the other hand, if the temperature decreases then a phase transition occurs to a lower-symmetry phase, for example a tetragonal or orthorhombic phase. The octahedral tilting is important to consider when calculating properties of the perovskites as it can affect for example the band gap and the energy of the material [4]. In the halide perovskites there are different phonon modes corresponding to octahedral tilting. For the simple perovskite special consideration will be taken to the M $(\frac{1}{2}, \frac{1}{2}, 0)$ and the R $(\frac{1}{2}, \frac{1}{2}, \frac{1}{2})$ tilting modes. There is a M mode corresponding to an in-phase tilting and a R mode which corresponds to out-of-phase tilting and they are demonstrated in Figure 2.5. [27].

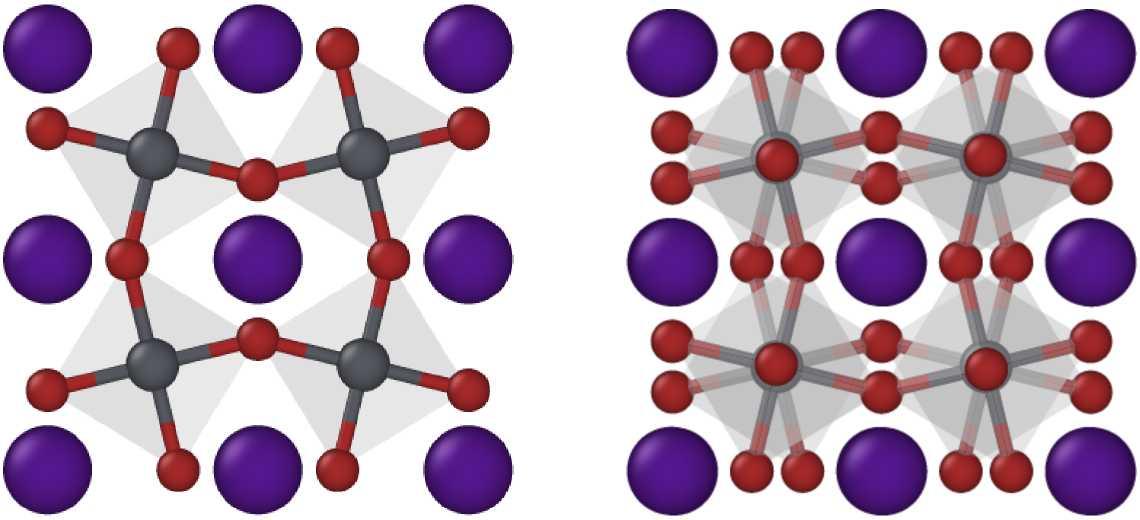

Figure 2.5: *Left*: Structure of the simple perovskite $CsPbBr_3$ in tetragonal phase and it corresponds to the M-mode in-phase tilting. *Right*: Structure of simple perovskite $CsPbBr_3$ in orthorhombic phase and it corresponds to the R-mode, out-of-phase tilting. Here, red is Br, blue is Cs and grey is Pb. The grey areas represent octahedra.

A commonly used tool to assess the structural stability of the material is to study whether two basic criteria are met, the Goldschmidt's tolerance factor and the octahedral factor. The Goldschmidt's tolerance factor, t, is a measure of the stability and distortion of crystal perovskite structures. It can also be used to calculate the compitability of an ion and a crystal structure and it is defined by the following equation,

$$t = \frac{r_A + r_X}{\sqrt{2}(r_B + r_X)}, \tag{2.9}$$

where r_A, r_B and r_X are the radii of the A-site cation, the B-site cation and the X-site anion, respectively. According to Yang *et al.* [4] values of t<1 correspond to octahedral tilting, due to the fact that the cation in the A-site is too small compared to the optimal size for bonding with the remaining atoms in the lattice. To obtain a stable perovskite material the value of the Goldschmidt's tolerance factor should have a value in the range of $0.81 \leq t \leq 1.0$. The octahedral factor, μ, is a second way of predicting the structure stability and is defined as

$$\mu = \frac{r_B}{r_X}. \tag{2.10}$$

To obtain stability in the perovskites, the octahedral factor should exceed 0.41 [2] [4] [5].

According to Lingyuan Gao *et al.* [11], the s orbital lone-pair electrons of the B-site ions play a large role in the different instabilities of the simple perovskites. Previously it was believed that only the distortions of the material due to off-centering motion of the B-site ion was a result of the aforementioned lone-pair electrons [10] but thanks to Lingyuan Gao *et al.* it is now clear that also the octahedral tilting can be described by the presence of lone-pair electrons. Hence, the instabilities of the material can not be described fully by only taking the tolerence factor and the octahedral factor into account. It is important to consider also the effect of the lone-pair electrons.

2.6.4 Polymorphous structures

The perovskites can, as many other crystal structures, be described by a monomorphous unit cell, for example the cubic cell, being repeated. This structure corresponds to the highest symmetry structure. If the atoms in a cubic cell are displaced slightly from their perfect positions and the structure is then relaxed it results in octahedral tilting and a polymorphous structure has been produced. According to previous studies, calculations of the band gap and other properties of the material can show variations from experimental values when a monomorphous structure is used. If, however, a polymorphous structure is used for such calculations, the results agree to a greater extent with the experimental results [29]. According to Zhao *et al.* the difference in band gap and in energy considering a monomorphous and a polymorphous structure can reach 0.5 eV and 20 meV/atoms respectively.

2.7 Phonons

Phonons are quantized vibrations of the atoms in a material and can, just as photons, be described both as a wave and a particle. Considering the wave analogy of phonons, the frequency of the wave, $\omega(k)$, is a function of the wave vector k and

$\omega(k)$ is known as the phonon dispersion relation. The wave vector is obtained by $k = 2\pi/\lambda$ where λ is the wavelength of the wave. In order to understand the phonon dispersion relation and how it is obtained it is helpful to analyze an infinite chain of atoms. First, let's consider an atomic chain with one atom in each unit cell. Of course, the atoms can move about their equilibrium positions and thereby exert forces on their neighbouring atoms. To easily describe how the atoms behave when affected by forces they can be considered to be connected to their neighbours with an imaginary spring of an atom-specific force constant, C. An equation of motion can be derived for an atom n by considering the positions of its neighbouring atoms,

$$m\frac{d^2u_n}{dt^2} = -C(u_n - u_{n-1}) + C(u_{n+1} - u_n), \tag{2.11}$$

where m is the mass of the atom and u is the displacement of the corresponding atom. This equation of motion may be solved by assuming a wave solution,

$$u_n(t) = ue^{i(kan-\omega t)}. \tag{2.12}$$

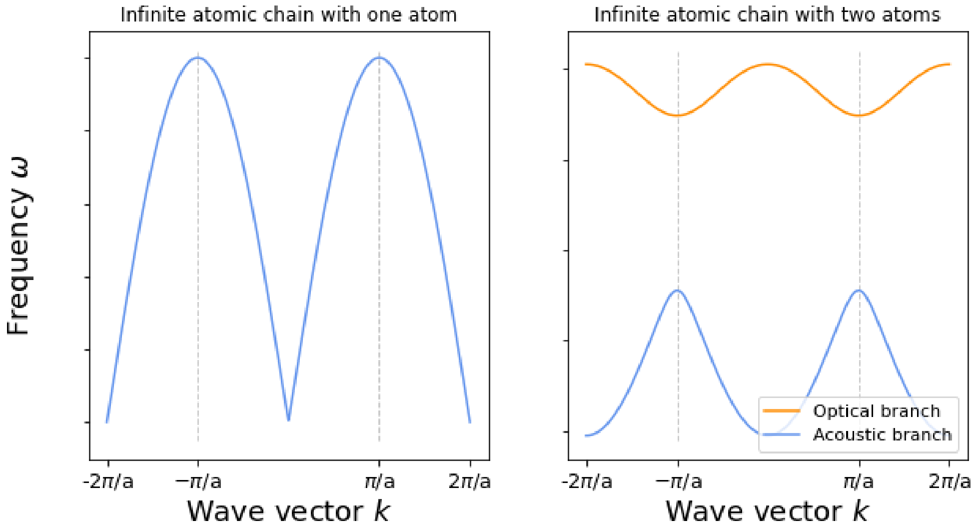

Figure 2.6: *Left:* Phonon dispersion of an infinite atomic chain with a one atom unit cell. The Brillouin zone is demonstrated by two vertical dashed lines.
Right: Phonon dispersion of an infinite atomic chain with a two atoms unit cell. The orange graph corresponds to the optical branch and the blue represents the acoustic branch. The Brillouin zone is demonstrated by two vertical dashed lines.

This wave is only defined in the lattice sites and has the frequency ω and the wave vector k. a corresponds to the distance between two neighbouring atoms and n is, as mentioned earlier, the number of the atom under consideration. Equation 2.11 can be solved by insertion of Equation 2.12 and from the solution the phonon dispersion relation is extracted,

$$\omega(k) = 2\sqrt{\frac{C}{m}}|\sin(\frac{ka}{2})|. \tag{2.13}$$

The phonon dispersion relation for an infinite atomic chain is visualized in Figure 2.6 and it describes waves propagating along the chain of atoms. When the structures of atoms become more complicated there can be several solutions to the equations of motion and each solution is called a normal mode. The excitation of each mode can be represented by a phonon.

We can now assume that there are two different kinds of atoms per unit cell in the considered infinite chain. The calculations to obtain the phonon dispersion relation are similar to the previous case. The lattice constant is now b which means that two neighbouring atoms are seperated by a distance of $b/2$ and the masses of the atoms are m_1 and m_2. Solving the equation of motions as above the following phonon dispersion relation is obtained:

$$\omega^2 = C\left(\frac{1}{m_1}+\frac{1}{m_2}\right) \pm C\left(\left(\frac{1}{m_1}+\frac{1}{m_2}\right)^2 - \frac{4}{m_1 m_2}\sin^2(\frac{kb}{2})\right)^{1/2}. \tag{2.14}$$

This dispersion relation will result in two normal branches, one acoustic and one optical branch. The acoustic branch corresponds to the propagation of sound in the material.

The phonons are, as mentioned earlier, quantized vibrations of the atoms in a material and hence the energies of phonons are quantized. The energy levels are defined as

$$E_l(k) = \left(l+\frac{1}{2}\right)\hbar\omega(k), \tag{2.15}$$

where l =1,2,3,... Both l and k can be treated as quantum numbers and they can be understood as the normal mode k that is excited to the level l. So far the phonons have been described using waves but it is also possible to describe them as particles. Instead of imagining waves moving through the material, each mode can be considered a particle. When studying for example thermal conductivity it is helpful to consider particles being generated in the hot end of a stick and then conducted towards the cold end [16].

3

Methods

3.1 Density functional theory

When simulating and modelling atoms and molecules it is desirable to solve the Schrödinger equation which governs the wavefunctions of the particles in the system. The Schrödinger equation is defined in Equation 2.1 and contains all information about the system in question. When considering a more complex system the parameters are too many for the Schrödinger equation to be solved analytically and numerical methods and approximations need to be included in the solution. A convenient way of solving the Schrödinger equation is to use the Density Functional Theory (DFT).

3.1.1 Approximations

In order to simplify the calculations of the Schrödinger equation, DFT takes advantages of several approximations. The Born-Oppenheimer approximation is utilized, where the ions in the system can be considered fixed in position compared to the much faster electrons. Therefore it is possible to decouple the dynamics of the ions and the electrons by expressing the wavefunction in terms of the positions of the ions and the positions of the electrons,

$$\Psi_{\text{total}} = \Psi_{\text{electrons}}\Psi_{\text{ions}}. \tag{3.1}$$

This leads to the assumptions that the wavefunctions depend only on the positions of the ion and not the velocity and that the electrons are only seen as a smeared out potential from the view of the ions. Another approximation that DFT makes use of is the mean-field approximation. Here, each particle is treated in an average potential of the remaining particles. It also approximates a many-body wavefunction with several single-particle wavefunctions,

$$\Psi(\mathbf{r}_1, \mathbf{r}_2, ..., \mathbf{r}_n) = \phi_1(\mathbf{r}_1)\phi_2(\mathbf{r}_2)...\phi_n(\mathbf{r}_n). \tag{3.2}$$

The single-particle wavefunctions are considered non-correlated. If this equation above is combined with the Schrödinger equation the following expression is obtained

$$H\phi_j(\mathbf{r}_j) = E\phi_j(\mathbf{r}_j), \tag{3.3}$$

where $j = 1, 2, ..., n$ corresponds to different particles. However, what makes DFT superior is that is uses the results of Hohenberg and Kohn.

3.1.2 Hohenberg-Kohn theorem

Hohenberg and Kohn proved two theorems which have become the basis of the density functional theory. The first theorem claims that the ground state electron density uniquely determines the external potential, or the positions of the ions. This means that if the ground state density of the electrons is known the ground state wavefunctions can be obtained as well.

Based on this first theorem it is also possible to connect the energy of the system and the electron density. The total energy of a many-electron system can be obtained through

$$E =< \Psi|H|\Psi >= \int d\mathbf{r}_1 ... d\mathbf{r}_n \Psi^*(\mathbf{r}_1, ..., \mathbf{r}_n)\hat{H}\Psi(\mathbf{r}_1, ..., \mathbf{r}_n), \tag{3.4}$$

where E is the total energy, H is the Hamiltonian and Ψ is the wavefunction. The Hamiltonian is here given by

$$\hat{H}(\mathbf{r}_1, ..., \mathbf{r}_n) = -\sum_i \frac{1}{2}\nabla_i^2 + \sum_i V_N(\mathbf{r}_i) + \frac{1}{2}\sum_{i\neq j}\frac{1}{|\mathbf{r}_j - \mathbf{r}_i|}, \tag{3.5}$$

where the first term is the kinetic energy of the electrons, $V_N(\mathbf{r}_i)$ is the Coulomb potential of the nuclei experienced by the orbiting electrons and the last term represents the interaction between the electrons. When studying the Hamiltonian above it is appearent that the energy is not dependent on the specific material but on the changes in the many-body wavefunction. This may be expressed as the energy E being a functional of the wavefunction Ψ. Combining this statement with the first theorem the ground state energy of the system, E, can be expressed as functional of the electron density $n(\mathbf{r})$,

$$E = F[n(\mathbf{r})]. \tag{3.6}$$

Instead of considering a many-body wavefunction, $\Psi(\mathbf{r}_1, ..., \mathbf{r}_n)$, of $3n$ variables (three dimensions for each particle) in order to obtain the ground state energy it is now only necessary to consider the electron density with solely three dimensions. However, to obtain the energies corresponding to the excited states the full many-body wavefunction is required [13].

The second theorem asserts that the ground state energy indeed is the lowest energy using the variational principle. The energy can be minimized by varying the electron density to find the ground-state energy and then other properties can be calculated [7].

3.1.3 Kohn-Sham equations

From the Hohenberg-Kohn theorem it is known that the ground state energy of many electrons is a functional of the electron density. However, the theorem does not give any suggestions of how the functional is to be constructed, but since the emergence of the Hohenberg-Kohn theorem several attempts to develop an expression for the functional have been made. Given the first Hohenberg-Kohn theorem the functional can be written as follows,

$$F[n] = \int n(\mathbf{r})V_n(\mathbf{r}) + < \Psi[n]|\hat{T} + \hat{W}|\Psi[n] > . \tag{3.7}$$

The first term, containing the external potential, is explicitly dependent on the electron density while the dependency on the remaining two, the kinetic energy and the Coulomb energy, is implicit. Kohn and Sham made the ansatz of replacing the original many-body problem with a system containing auxiliary non-interacting particles. They assumed that the ground state density of the original system is equal to the system of the non-interacting particles, which is exactly soluble.

The Hamiltonian of the auxiliary system split the implicit term in Equation 3.7 into two terms, a kinetic energy term and a Coulomb energy term. There is also a term corresponding to the interaction between the particles and an additional term which represents the difference in energy between the total energy and energy calculated using the functional of the electron density. The expression for calculating the energy of the system using a functional of the electron density, which includes the single-body wavefunctions, or Kohn-Sham orbitals, ϕ_i can now be written as following:

$$\begin{aligned} E &= F[n] \\ &= \int d\mathbf{r} n(\mathbf{r})V_n(\mathbf{r}) - \sum_i \int dr \phi_i^*(\mathbf{r})\frac{\nabla^2}{2}\phi_i(\mathbf{r}) \\ &+ \frac{1}{2}\int\int d\mathbf{r}d\mathbf{r}'\frac{n(\mathbf{r})n(\mathbf{r}')}{|\mathbf{r}-\mathbf{r}'|} + E_{xc}[n]. \end{aligned} \tag{3.8}$$

The total energy is constituted of the external potential V_n, the kinetic energy of the electrons, the Hartree energy (the interaction between electrons) and the additional energy mentioned above which is called the exchange-correlation energy. If the exchange-correlation energy, E_{xc}, was known then it would be possible to calculate the total energy of the system using the electron density.
Hohenberg and Kohn were also known for the *Hohenberg-Kohn variational principle* which can be expressed as

$$\frac{\delta F[n]}{\delta n} = 0 \text{ at } n_0, \tag{3.9}$$

where n_0 is the ground-state density. Given Equation 3.9 one can obtain equations for the single-body wavefunctions of the particles. Provided that the wavefunctions are orthogonal, one can utilize the variational principle from equation 3.9 to obtain the *Kohn-Sham equations*,

$$\left(-\frac{1}{2}\nabla^2 + V_n(\mathbf{r}) + V_H(\mathbf{r}) + V_{xc}(\mathbf{r})\right)\phi_i(\mathbf{r}) = \epsilon_i\phi_i(\mathbf{r}). \tag{3.10}$$

The first three terms in the equation above correspond to the kinetic energy of the auxiliary particles, the external potential and the Hartree potential. The last potential term is the exchange-correlation potential and is given by

$$V_{xc} = \frac{\delta E_{xc}[n]}{\delta n}. \tag{3.11}$$

How well the functional $E_{xc}[n]$ is approximated determines the accuracy of the DFT calculations [13].

3.1.4 Exchange-Correlation functionals

In order to complete the density functional theory the exchange-correlation functional needs to be approximated. As the exchange-correlation potential is small compared to the kinetic potential and the Hartree potential, it may be expressed sufficiently well as a local, or nearly local, functional of the electron density, $n(\mathbf{r})$. The local density approximation (LDA) is one of the more simple approaches to obtain a form for the functional. This approximation assumes that the electronic structure in solid materials can be described by a homogeneous electron gas. When making this assumption the exchange and correlation functional depends only on the electron density in each point, i.e. it can be seen as local. The exchange-correlation functional, when approximated with LDA, can be expressed as

$$E_{xc}^{LDA}[n(\mathbf{r})] = \int d\mathbf{r} n(\mathbf{r})\epsilon_{xc}(n(\mathbf{r}))), \tag{3.12}$$

where ϵ_{xc} is the energy density per electron at a point $\mathbf{r}$. LDA has inspired several other, more complicated, approximations such as the Generalized Gradient Approximation (GGA). GGA takes the electron density inhomogeneity that occurs in real materials into account. In addition to include the local density in the approximation, GGA also introduces the gradients of the density [18],

$$E_{xc}^{GGA}[n(\mathbf{r})] = \int d\mathbf{r} n(\mathbf{r})\Delta n(\mathbf{r})\epsilon_{xc}(n(\mathbf{r})). \tag{3.13}$$

A modification to the GGA is the meta-GGA which considers the kinetic energy density, and by extension the Kohn-Sham orbitals, as well. One of the functionals in the meta-GGA family is Strongly Constrained and Appropriately Normed functional (SCAN) and this functional has in several tests shown superiority over other functionals [28].

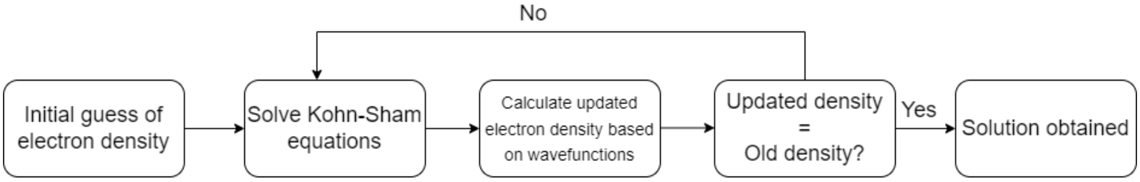

Figure 3.1: Scheme showing the principles of the self-consistent calculations loop in DFT.

3.1.5 Self-consistent calculations

The questions remaining are how to solve the Kohn-Sham equations and how to obtain the total energy when the Kohn-Sham equations are solved. This is not a straightforward task because the Hartree potential, V_n, and the exchange-correlation potential, V_{xc}, in Equation 3.10 depend on the electron density, $n(\mathbf{r})$, which depends on the unknown single-particle wavefunctions ϕ_i through

$$n(\mathbf{r}) = \sum_i |\phi(\mathbf{r})|^2. \tag{3.14}$$

This means that each solution ϕ_i depends on all other solutions ϕ_j and a self-consisting loop is required in order to obtain a solution. The procedure which is used when DFT is employed to solve the Kohn-Sham equations is to guess an electron density, $n(\mathbf{r})$, which is inserted in Equation 3.10 where the wave functions ϕ_i are obtained. Using Equation 3.14, an updated electron density is obtained and compared with the initial one. If the densities are similiar within a certain tolerance the loop is exited and the solutions of the Kohn-Sham equations are obtained. However, if this is not the case the density is once again inserted in the Kohn-Sham equations and the self-consistent calculations carry on. A schematic of this procedure is visualized in figure 3.1 [13].

4

Computational details

In order to better understand the halide double perovskites, several of their properties were studied during this thesis. Previous studies on single perovskites have been conducted in order to analyze the difference in energy and band gap between the monomorphous structure and the polymorphous structure of the simple halide perovskites. It was found that the size of the band gap increases and the total energy decreases significantly when analyzing the properties using a polymorphous structure as opposed to a monomorphous structure [29]. However in the beginning of this thesis, when studying the same properties of the double perovskite $Cs_2AgBiBr_6$, the differences in energy and band gap between the two structures were found to be much less prominent. Also the tilting of the octahedrals in the material was much less prominent in the double perovskite compared to the simple one. It was therefore decided to perform further studies to better understand this phenomena. To be able to study the tilting in more detail, phonon dispersions were calculated for the materials $Cs_2AgBiBr_6$ and $CsPbBr_3$ and several imaginary modes, corresponding to phonon instabilities in the material, were found. The potential energies were calculated along the imaginary modes and then visualized in plots against the displacement of the atoms compared to a cubic structure. These plots resulted in an indication of the tilting in the materials. The potential energy landscape was calculated for several different halide double perovskites in order to examine whether reduced octahedal tilting, compared to the simple perovskites, is a general trend in all halide double perovskites.

4.1 Selection of parameters

4.1.1 Convergence tests

Prior to calculations, convergence tests were performed to obtain optimal values of some of the relevant parameters. The total energy of the system was calculated repeatedly while one parameter was altered and the other ones were kept fixed. When the energy converges within a chosen limit at a value of a parameter, then good enough accuracy has been achieved. The cutoff energy and the number of k-points to be used to sample the Brillouin zone were the two parameters which were altered until convergence. The convergence limit was set to 1 meV/atom. The different cutoff energies tested ranged from 200 eV to 1200 eV and the k-point grids which were tested are $2 \times 2 \times 2$, $4 \times 4 \times 4$, $6 \times 6 \times 6$, and $8 \times 8 \times 8$. The optimal cutoff energy and number of k-points are different for each studied material.

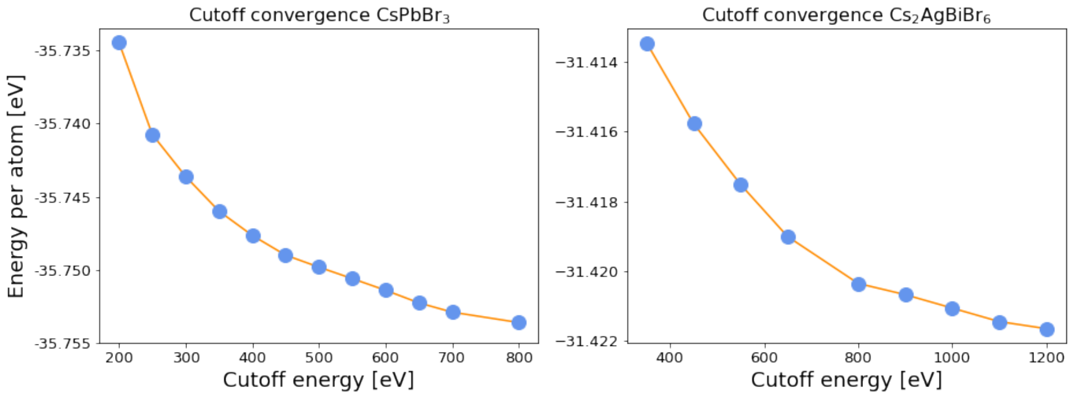

Figure 4.1: Cutoff energy convergence tests for the simple perovskite $CsPbBr_3$ and the double perovskite $Cs_2AgBiBr_6$ using VASP.

The results of the convergence tests for the simple perovskite, $CsPbBr_3$, and the double perovskite, $Cs_2AgBiBr_6$, are visualized in Figure 4.1. The convergence limit of 1 meV/atom was fulfilled at 450 eV for $CsPbBr_3$ and 800 eV for $Cs_2AgBiBr_6$. These values were used as guidelines in the choice of the optimal cutoff energies. After further convergence tests considering the entire phonon spectra and examinations of the computational costs that comes with higher accuracy, the cutoff energies 700 eV and 750 eV were chosen for $CsPbBr_3$ and $Cs_2AgBiBr_6$ respectively. These values were used throughout the thesis if nothing else is mentioned.

4.1.2 DFT and VASP specific parameters

The energies and forces were calculated with DFT using the VASP software package. In VASP, the quantities such as the electronic charge density and the local potentials are expressed in a plane wave basis set and the interactions between particles involved are described using the projector-augmented-wave (PAW) method. When it comes to determining the electronic groundstate of a system, VASP uses iterative matrix diagonalization techniques, such as RMM-DIIS or blocked Davidson algorithms.

When using DFT to solve the Schrödinger equation approximately, there are two self-consistent loops. One loop where electronic self-consistency steps are performed until energy convergence and a second loop where the positions of the ions are updated until energy convergence. The parameters NELM and NELMIN define the maximum and minimum numbers of electronic self-consistency steps and NSW dictates the number of ionic steps. During this thesis the following values were used: NELM=120, NELMIN=4 and NSW=100 when ionic relaxation was required, otherwise NSW=0 [25].

DFT calculations require a functional which relates the energy of the system, E, to the electron density, $n(\mathbf{r})$. The functional used for the calculations within this thesis is the meta-GGA functional SCAN (Strongly Constrained and Appropriately

Normed) which is a semilocal density functional. SCAN was selected based on a previous work evaluating how well a functional is suited for a particular material. In that study, various functionals were benchmarked against a higher level method, Random Phase Approximation (RPA), and SCAN resulted in the best agreement [6].

The calculations in this thesis were, if nothing else is specified, performed using the VASP software package which is employing DFT to obtain energies, forces and to relax structures. When running calculations using VASP, four input files are required; the POSCAR includes the positions of the atoms, the POTCAR file contains the pseudopotential for each atom species, KPOINTS defines the number of k-points used to sample the Brillouin zone and INCAR is the central input file which defines *what to do* and *how to do it.* The INCAR file includes several parameters which need to be defined properly in order to decrease the computational cost and to increase the accuracy of the calculations. The INCAR file used can be found in Appendix. In the KPOINTS file the type of grid used for the calculations is defined as a Γ-centered grid, which reduces the computational cost compared to other grids [25].

The parameter EDIFF specifies when to break the electronic self consistency-loop and it was set to break when the difference in energy between two consecutive iterations was $1e^{-5}$ eV. KPAR is the parameter which determines the number of k-points to be treated in parallel. For most of the calculations two k-points are treated in parallel. A number of bands can also be treated in parallel and this number is defined by the parameter NPAR and is optimally given by $\sqrt{\#cores}$. The value NPAR=2 was used for the simpler calculations and NPAR=8 for the larger ones. The parameter ISIF was set to 3 and this implies that both the stress tensor and forces were calculated and that the positions of the atoms, the cell shape and the cell volume are allowed to change.

4.2 Energy and band gap analysis

In order to study the band gap and energy of the structure, a convergence test was done for the material $Cs_2AgBiBr_6$ on the CP2K software package. A cutoff energy of 400 eV and a relative cutoff of 60 eV were selected for the calculations of the band gap and density of states. The parameter run type was set to GEO_OPT, which sets the type of run to Geometry Optimization. Two files containing information about the band gap and the density of states were produced using the CP2K software and these files were visualized using Python.

In order to study the effect of polymorhous structures compared to monomorphous structures, energy relaxations of a system of 320 atoms were performed. The relaxations were done on a monomorphous structure and a polymorphous structure of a cubic phase. The polymorphous structures were produced using a Python script randomly displacing the atoms. Several calculations were done for the polymorphous structures, and the displacement of the atoms ranged from 0.087 Å to 0.7 Å. The energies resulting of the polymorphous calculations were visualized compared to the energies of the monomorphous structure.

4.3 Phonon analysis

The phonon dispersions of the materials were produced using the python package Phonopy together with VASP. A Phonopy script was used to produce POSCARs with different atomic positions given a reference POSCAR that had been relaxed in regard to energy and cell shape and size. The forces were calculated for the produced POSCARs without performing any ionic relaxation. The structures consisted of 40 atoms. From the calculated forces the phonon dispersion could be obtained by running a python script that used the Phonopy function *get_band_structure*. The phonon dispersions of the perovskites were visualized along the path $\Gamma \rightarrow X \rightarrow M \rightarrow \Gamma \rightarrow R \rightarrow X$. The path was chosen by usage of the ASE function *special_points*. It returns the optimal k-points for that specific structure.

The phonon dispersion relations showed imaginary modes, which correspond to instabilities in the material, at certain high-symmetry points. To analyze these imaginary modes further, potential energy landscapes were produced along these phonon modes. This was done by visualizing the free energy of the system at different displacements of the atoms compared to their cubic positions.

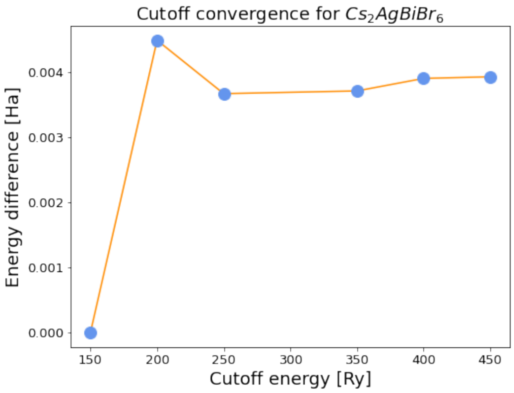

Figure 4.2: Cutoff energy convergence for $Cs_2AgBiBr_6$ using CP2K.

To make sure that the true energy minimum structure is found, relaxation of a structure close to minimum energy was conducted in VASP. Interpolation was then conducted between the true minimum structure and the cubic structure. A number of POSCARs were created between the cubic structure and the relaxed one and the energy of each structure was calculated. This last step may be done easily for several materials. A python script which exchanges atoms in POSCARs was used to create new materials and the new structures were then relaxed in order to be able to obtain new potential energy landscape for many materials. The python function *spglib.get_spacegroup* was used to identify the space groups of the structures along the energy landscapes.

4.4 Choice of materials

The materials which were analyzed are $Cs_2AgBiBr_6$, $Cs_2AgGaBr_6$ and $Cs_2InBiBr_6$. $Cs_2AgBiBr_6$ was chosen for further examination due to its favorable band gap for optoelectronic applications and because of many successful attempts to produce highly stable thin films of that material [14] [17] [12]. The Goldschmidt tolerance factor, expressed in equation 2.9, for $Cs_2AgBiBr_6$ is 0.84 [26]. This value corresponds to octahedral tilting and is in the range of values resulting in stable perovskites, which are two criteria for the choice of material. The remaining two materials were chosen based on the number of cations with lone-pair electrons. $Cs_2AgBiBr_6$ has one ion with lone-pair of electrons , $Cs_2InBiBr_6$ has two and $Cs_2AgGaBr_6$ has none.

4.5 Spin-orbit coupling

The effect of spin-orbit coupling on the calculations of the energy of the material $Cs_2AgBiBr_6$ was studied as well. This was done by adding the parameter LSORBIT=.TRUE. to the INCAR. Spin-orbit coupling is included in the calculations by adding an extra term to the Hamiltonian, $H_{\text{SOC}} \propto \vec{\sigma} \cdot \vec{L}$, where $\vec{\sigma}$ is the Pauli-spin operator and $\vec{L} = \vec{r} \times \vec{p}$ is the angular momentum operator. Now, the direction of the magnetic moment is taken into account when calculating the energy of the system. An interpolation between the cubic structure and the tetragonal structure was performed, including the effect of spin-orbit coupling when calculating the energies.

5

Results and Discussion

5.1 The halide simple perovskite $CsPbBr_3$

When studying the phonon dispersion of the halide simple perovskite $CsPbBr_3$, imaginary modes are found at the M- and R-symmetry points, which correspond to the **k**-values of ($\frac{1}{2}$,$\frac{1}{2}$,0) and ($\frac{1}{2}$,$\frac{1}{2}$,$\frac{1}{2}$). The phonon dispersion relation is visualized in Figure 5.1. At the R-symmetry point there are two degenerate imaginary modes and at the M-symmetry point there is one single imaginary mode. The imaginary modes are analyzed further by calculating the energies of the structures along them. The structures are relaxed and interpolation is performed using the cubic and the relaxed structure. Further information concerning the interpolation process is found in Section 4.3. From this, anharmonic potential wells are produced which indicate the optimal shape of the structures corresponding to both imaginary modes. These potential energy surfaces are depicted in Figure 5.2. The minimum energies of the systems are found at a displacement of 0.7 Å, where the displacement given is the smallest possible displacement between the structure in question and the cubic structure. The energy difference between the cubic structure and the lowest-energy structure is 12 meV per atom for both modes. These low-symmetry structures correspond to the tetragonal phases I4/mcm (140) and P4/mbm (127). The Goldschmidt tolerance factor is given by Equation 2.9 and is, for this material, calculated to the value of 0.81.

5.2 The halide double perovskites

5.2.1 $Cs_2AgBiBr_6$

Based on the results from Zhao *et al.* [29] described in section 2.6.4, where the calculations of the properties of the simple perovskite using a monomorphous cubic structure deviate from experimental results, the band gaps and energies of the double perovskite $Cs_2AgBiBr_6$ were calculated for a monomorphous and polymorphous cubic structures. Eight independent calculations were performed using the polymorphous structure and the results are visualized in Figure 5.3. The graph to the left shows the band gaps of the independent runs using the polymorphous structure together with a mean value for the different calculations and the value of the band gap corresponding to the monomorphous structure. The difference between the band gaps of the monomorphous structure and the polymorphous calculations is 0.058 eV. The energy of the system is visualized in the graph to the right. The value of the

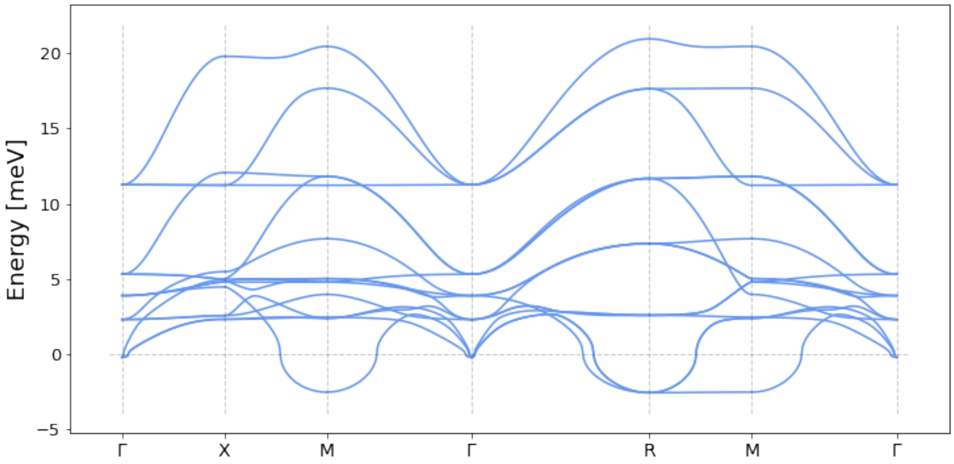

Figure 5.1: Phonon dispersion relation corresponding to $CsPbBr_3$. One imaginary mode is found at the M-symmetry point and one degenerate mode at the R-symmetry point.

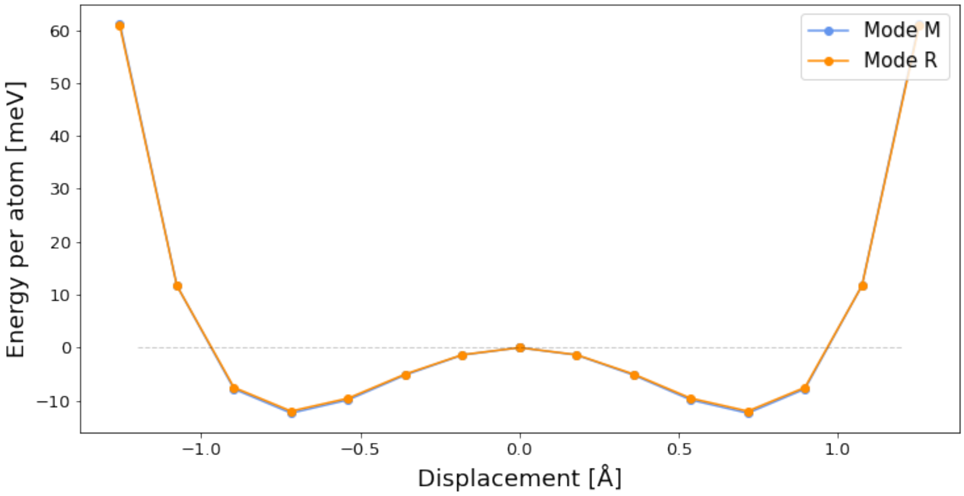

Figure 5.2: Potential energy surfaces along the imaginary modes of the R- and M-point of $CsPbBr_3$.

energy calculated from the monomorphous structure has been subtracted from the energies, resulting in an energy difference of the independent polymorphous runs and the monomorphous structure. This energy difference is 0.0084 eV per atom. Comparing these values to the ones corresponding to the simple perovskite which are mentioned in Section 2.6.4, the difference is significantly smaller for the double perovskite.

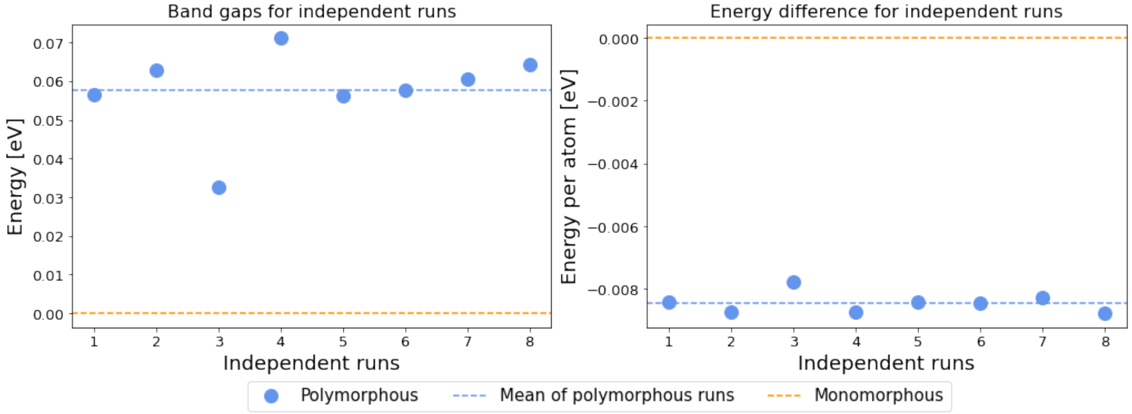

Figure 5.3: Differences in energy and band gap between the monomorphous and the polymorphous structures of $Cs_2AgBiBr_6$.

The phonon dispersion relation for the double perovskite $Cs_2AgBiBr_6$ shows imaginary modes corresponding to instabilities at the Γ- and X-symmetry points, as depicted in Figure 5.4. The two imaginary modes at the Γ-symmetry point are triply degenerate and these modes correspond to the R- and M-modes of the simple perovskite folded onto the Γ-point. As the R- and M-modes are connected to the octahedral tilting in the material, these two degenerate modes will be analyzed further and the mode at the X-point will not be treated in the scope of this thesis. The potential energy surfaces corresponding the the two degenerate modes at the Γ-symmetry point are pictured in Figure 5.5, where mode 1 represents the modes of lower energy in the phonon dispersion spectrum and mode 2 the modes of higher energy. Mode 1 has a well-depth of 0.19 meV per atom where the minimum energy is found at a displacement of 0.23 Å and the structure corresponding to the minimum energy is tetragonal of space group I4/m (87). The second mode on the other hand has its minimum energy of -0.034 meV per atom at a displacement of 0.13 Å. This structure is orthorhombic and a member of the space group Pnnn (48). The most stable mode of the two is the tetragonal mode because it shows a deeper energy well and this agrees with the experimental phase of the material being tetragonal as well [20]. The Goldschmidt tolerance factor is 0.84.

In the continuation of this thesis only the lowest-energy mode will be analyzed further. This is due to the limited period of time and because of the assumption that this property of reduced tilting is true for all modes in the relevant materials, just as it is for $Cs_2AgBiBr_6$.

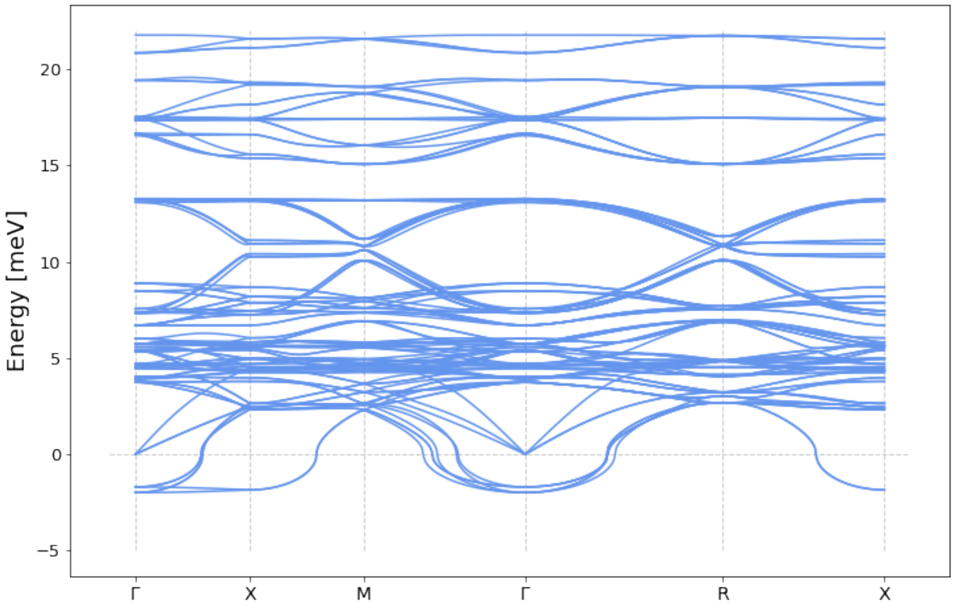

Figure 5.4: The phonon dispersion relation corresponding to $Cs_2AgBiBr_6$. One degenerate imaginary mode is found at the X-symmetry point and two triply degenerate imaginary modes at the Γ-symmetry point.

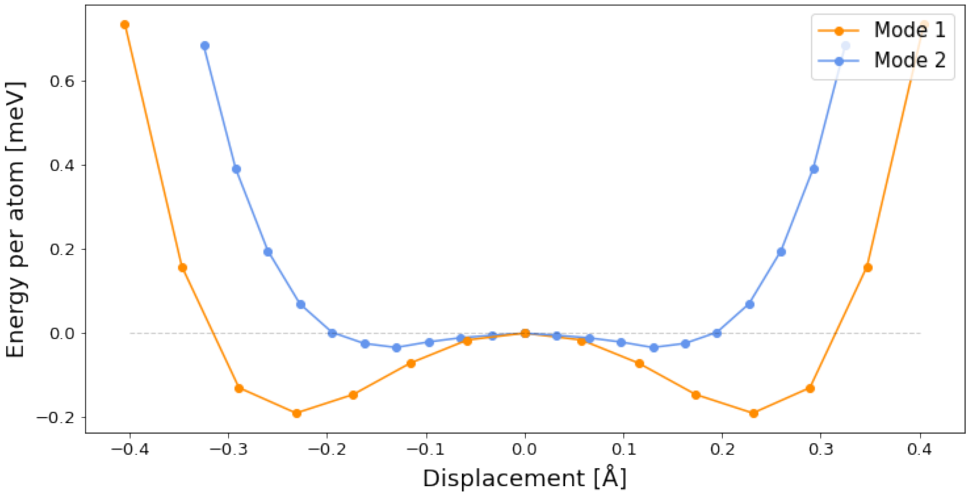

Figure 5.5: Potential energy surfaces corresponding to the two imaginary modes at the Γ-symmetry point of $Cs_2AgBiBr_6$.

5.2.2 $Cs_2InBiBr_6$

The potential energy surface corresponding to the material $Cs_2InBiBr_6$ is visualized in Figure 5.6. For the first mode of this material the depth of the well is 5.1 meV per atom and the structure at a displacement of 0.61 Å exhibits the lowest energy. The structure corresponding to this mode is tetragonal of space group I4/m (87) and the Goldschmidt tolerance factor for $Cs_2InBiBr_6$ is 0.79.

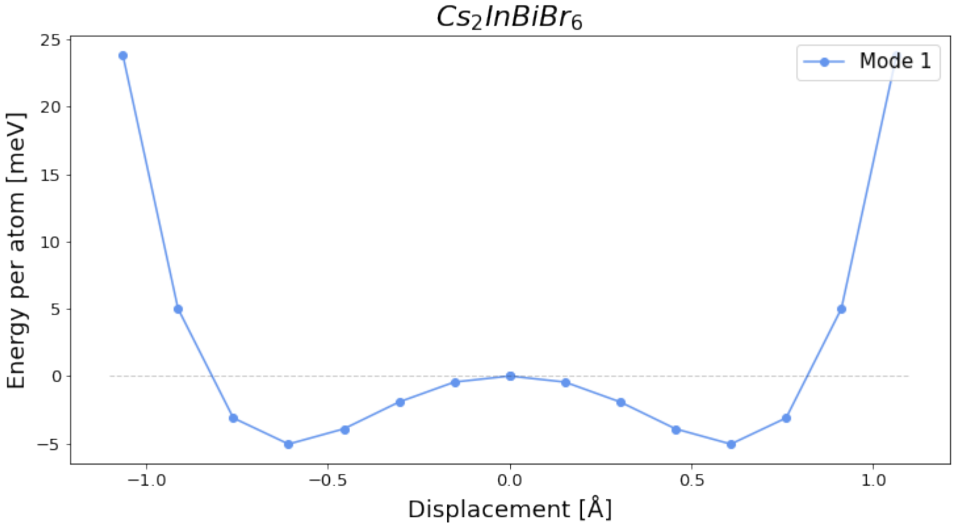

Figure 5.6: Potential energy surface corresponding to the lowest imaginary mode at the Γ-symmetry point of $Cs_2InBiBr_6$.

5.2.3 $Cs_2AgGaBr_6$

Considering the material $Cs_2AgGaBr_6$ in Figure 5.7, the potential energy surface shows different characteristics than the previous materials. The cubic phase of the material, corresponding to zero displacement of the atoms, represents the lowest-energy structure. As the structure approaches a tetragonal phase it increases in energy, resulting in the cubic phase being the most stable, when only considering the energy surface. The Goldschmidt tolerance factor is evaluated to the value of 0.81.

5.3 Effect of lone-pair electrons on octahedral tilting

In order to more easily compare the potential energy surfaces calculated for the materials listed above they are all visualized in Figure 5.8 and the width and depth of the energy wells are found in Table 5.1. From the mentioned graph it is obvious that there are large differences between the materials when it comes to the size and shape of the energy wells. The simple perovskite $CsPbBr_3$ and $Cs_2InBiBr_6$ have

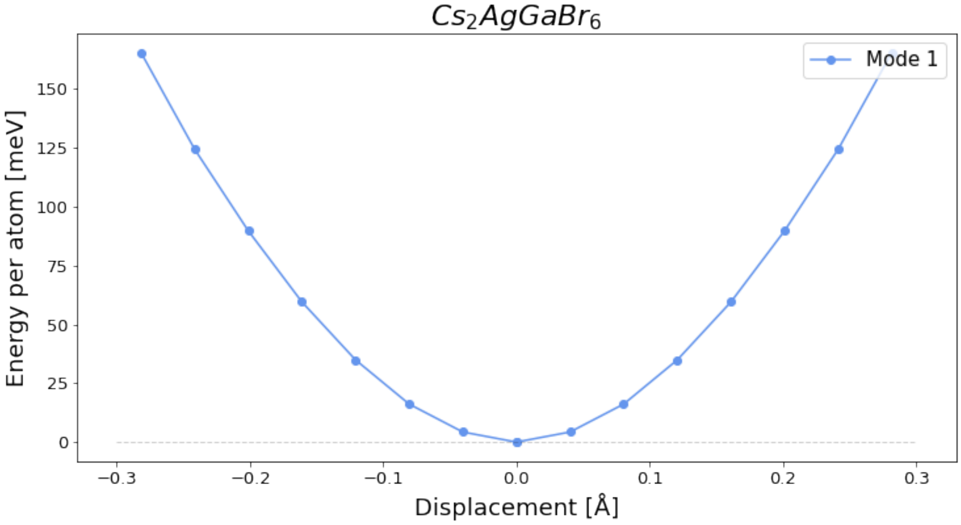

Figure 5.7: Potential energy surface corresponding to lowest imaginary mode at the Γ-symmetry point of $Cs_2AgGaBr_6$.

the deepest wells, $Cs_2AgBiBr_6$ has a small well and the lowest-energy structure of $Cs_2AgGaBr_6$ corresponds to the cubic structure, i.e. it has no double well potential. The size of the energy well is, as mentioned earlier, an indication of the octahedral tilting in the material. Therefore it can be concluded that the $CsPbBr_3$ and $Cs_2InBiBr_6$ have stronger octahedral tilting than $Cs_2AgBiBr_6$. The final material $Cs_2AgGaBr_6$ does not show any tilting. In Figure 5.9 the lowest-energy structures of $Cs_2InBiBr_6$, $Cs_2AgBiBr_6$ and $Cs_2AgGaBr_6$ are visualized. Also in this figure it is clear that the tilting is more prominent in $Cs_2InBiBr_6$. $Cs_2AgBiBr_6$ shows a small amount of tilting and the final structure, $Cs_2AgGaBr_6$m exhibits no tilting. It can also be noticed that the lattice parameter of the structures decreases with the octahedral tilting.

The Goldschmidt tolerance factor of a material is usually used as a measure of the stability and distortion of the structure and is defined in Equation 2.9. If the value of the tolerance factor is smaller than 1 it is an indication of octahedral tilting. This would for example be the result of the Cs^+-ion being small compared to the rest of the ions. Considering the Goldschmidt tolerance factor of the mentioned materials it has similar values for all materials. The values are in the range of 0.79 to 0.84, which would suggest a similar degree of octahedral tilting for the different materials. Based on this result it can be concluded that the strength of octahedral tilting can not be predicted solely by a geometric model based on ionic effects.

However, this inconsistency may be explained by considering the results of Lingyuan Gao *et al.* described in Section 2.6.3. They claim that octahedral tilting in simple perovskites as well as off-centering of the B-ion can be induced by the lone-pair electrons of the B-site ions. Studying the ions used during this thesis they are Pb^{2+}, In^+ and Bi^{3+} which have one lone pair of electrons each while Ag^+ and Ga^{3+} do not.

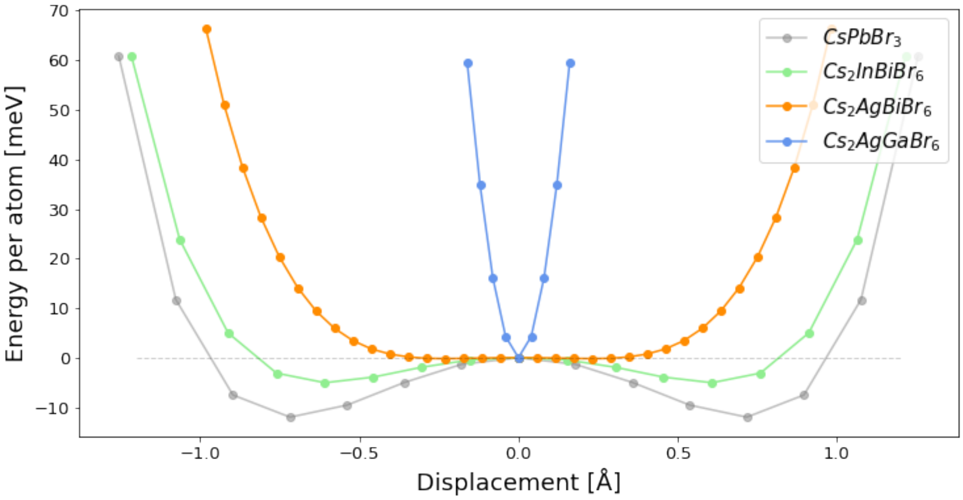

Figure 5.8: Potential energy surfaces corresponding to the lowest imaginary mode at the Γ-symmetry point of $Cs_2AgBiBr_6$, $Cs_2InBiBr_6$ and $Cs_2AgGaBr_6$ and the M-symmetry point of $CsPbBr_3$.

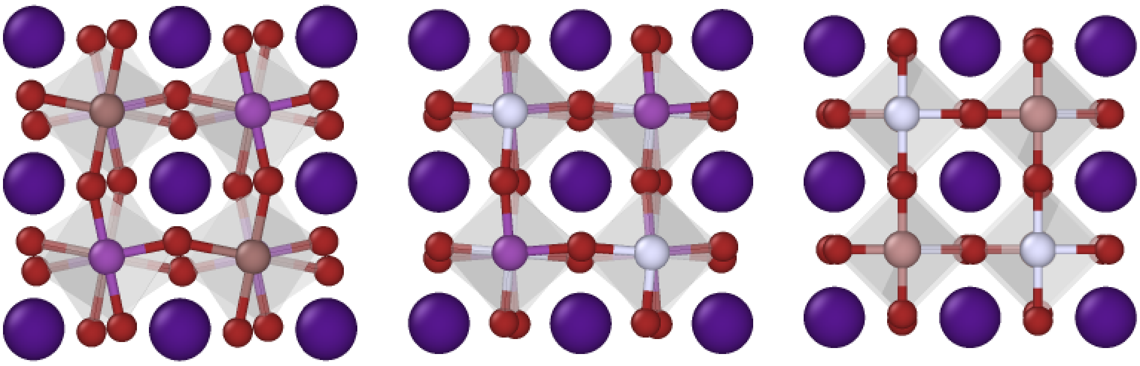

Figure 5.9: *Left*: Structure of $Cs_2InBiBr_6$ in tetragonal phase. *Middle*: Structure of $Cs_2AgBiBr_6$ in tetragonal phase. *Right*: Structure of $Cs_2AgGaBr_6$ in tetragonal phase. Here, red is Br, blue is Cs, grey is In, purple is Bi and white is Ag. The grey areas represent octahedra.

Material	E_{min} [meV]	Disp [Å]	Goldschmidt
$Cs_2AgBiBr_6$	0.19	0.23	0.84
$Cs_2InBiBr_6$	5.1	0.61	0.79
$Cs_2AgGaBr_6$	0	0	0.81
$CsPbBr_3$	12	0.7	0.81

Table 5.1: Properties corresponding to different perovskites. E_{min} is the energy difference between the cubic and the lowest energy structure and the displacement, in Å, represents where the lowest energy occurs.

Analyzing the materials in question further it can be noticed that the *B*-site ion of $CsPbBr_3$, which is Pb^{2+}, has lone-pair electrons and it has prominent octahedral tilting. This agrees with the result of Lingyuan Gao *et al.* Continuing to the double perovskites, $Cs_2InBiBr_6$ has lone-pairs on both *B*-site cations, $Cs_2AgBiBr_6$ has one *B*-site cations with a lone-pair and $Cs_2AgGaBr_6$ has no lone-pairs. Comparing the number of lone-pairs of electrons to the size of the energy wells of the materials there is a clear trend. $Cs_2InBiBr_6$, which has two lone-pairs, corresponds to the most prominent tilting while $Cs_2AgBiBr_6$ has one lone-pair of electrons and exhibit relatively small octahedral tilting. $Cs_2AgGaBr_6$ has no lone-pair electrons and shows no tilting as the cubic structure has the lowest energy.

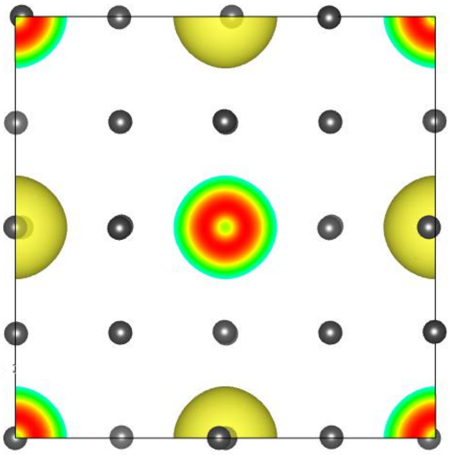

Figure 5.10: The spherical electron density of Bi^{3+}-ion corresponding to the lone-pair electrons.

There are also studies claiming that the position of the *B*-site ion can be distorted by lone-pair electrons [10]. Due to the large electronegativity of the lone-pair electrons belonging to an ion, the position of the ion in question as well as neighbouring ions may be distorted and this may cause changes in the properties of the material. The lone-pair electrons were identified for the material $Cs_2AgBiBr_6$ and the electron density corresponding to the lone-pair electrons of the Bi^{3+}-ions is visualized in Figure 5.10. As can be interpreted by the figure, the electron density of the lone-pair electrons of the Bi^{3+}-ion is spherical and hence the lone-pairs do not alter the position of the ion.

5.4 Effect of octahedral tilting on the band gap

The band gap of a material is obtained by calculating the difference in energy between the lowest state in the conduction band (CBM) and the highest state in the valence band (VBM). Therefore, in order to study the tuning of the band gap, the CBM and the VBM are important properties to examine. According to previous studies the band gap of a simple perovskite is dependent on the overlap of the antibonding orbitals of *B*-and *X*-site ions and the overlap can be tuned either by tilting of the octahedra or by changing the ions in the material [4]. First, the relationship between the octahedral tilting and the band gap is considered. Upon tilting, the overlap of the orbitals contributing to the VBM decreases, resulting in a lowering of the VBM which increases the band gap. Secondly, the overlap of atomic orbitals may be tuned by exchanging the ions which consequently alters the lattice parameter and the states forming the bonds. A smaller lattice parameter causes a larger overlap which decreases the band gap [19]. As the behaviour of the band gap of the double perovskites agrees with the simple perovskite, it is assumed that the orbitals combine in the same way and that this has the same effect on the band gap as in the simple perovskite case.

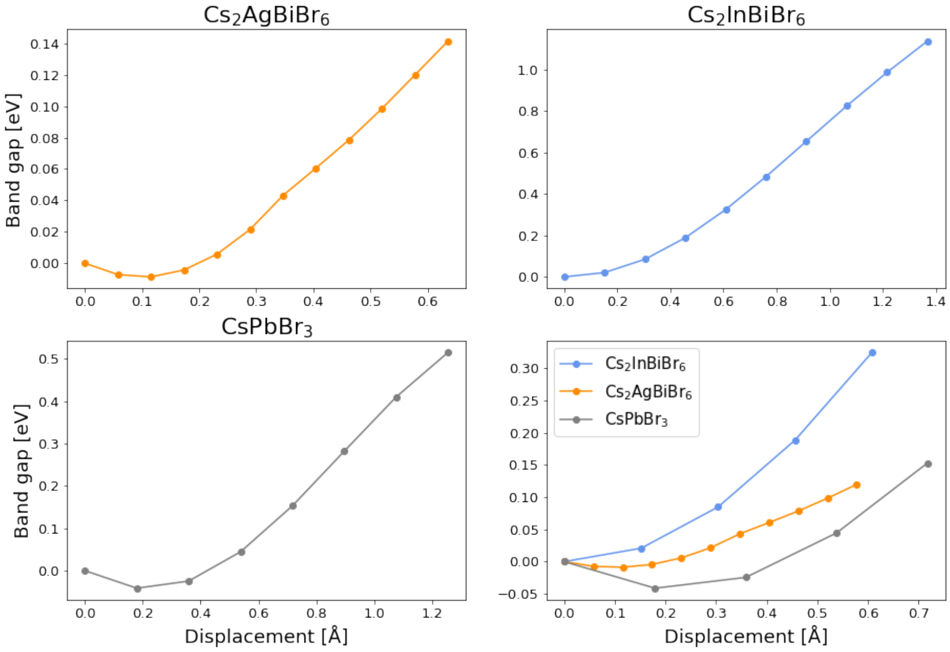

Figure 5.11: Band gaps corresponding to various perovskites at different levels of octahedral tilting.

The band gaps corresponding to double perovskite structures of different extent of octahedral tilting were obtained using the calculations from VASP. The exchange-correlation functional SCAN may underestimate the total band gap but the relative band gap variations should be reliable. The results for the materials $CsPbBr_3$, $Cs_2AgBiBr_6$ and $Cs_2InBiBr_6$ are visualized in Figure 5.11. The two latter materials, the double perovskites, exhibit similar behaviour for different levels of tilting which agrees with the results of the simple perovskite, both in this study and in previous ones. The size of the band gaps of these three materials increases as the octahedra tilt but the inclinations of the graphs are different. For $Cs_2AgBiBr_6$, $Cs_2InBiBr_6$ and $CsPbBr_3$ the inclinations of the linear parts of the slopes are estimated to 0.25 eV/Å, 0.91 eV/Å and 0.6 eV/Å respectively. This may be due to the different lattice parameters of the materials or the different states forming the antibonding overlapping orbitals.

5.5 Spin-orbit coupling

Calculations of band gaps at different displacements for the first mode of the material $Cs_2AgBiBr_6$ were conducted including the spin-orbit coupling effect. The results are visualized in Figure 5.12 as well as the energies and band gap variations calculated without the spin-orbit coupling. When it comes to the energy results, the structures of lowest energy have the same displacement for both calculations. However the relative energy of the system at this displacement is approximately 0.04 eV higher when including the spin-orbit coupling. Looking at the results of the band gap when including the spin-orbit coupling, the band gap variation increases for all displacements with approximately 1 meV. An interesting observation is that the band gap seems to decrease initially when the spin-orbit coupling is not included. When it is accounted for the band gap increases for all displacements.

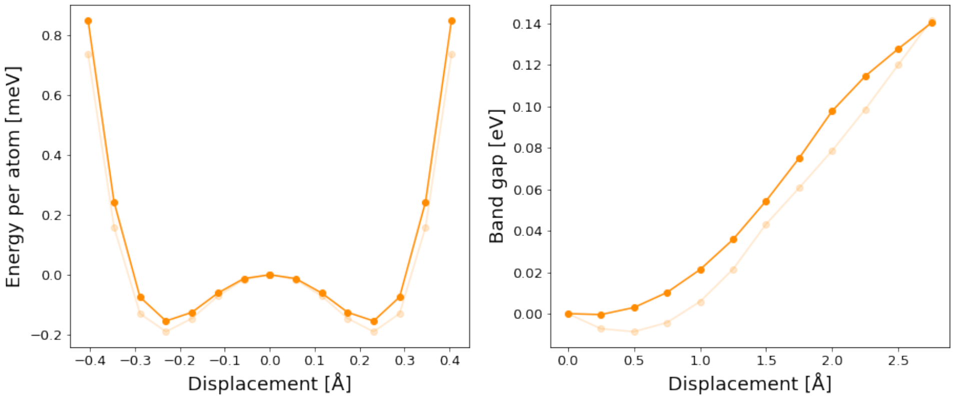

Figure 5.12: The results of the energy per atom and the band gap using the spin-orbit coupling are visualized for the material $Cs_2AgBiBr_6$. The results of not including the spin-orbit coupling are seen as transparent.

6

Conclusion

In this thesis the effect of dynamical disorder on the structure and electronic properties of halide double perovskites was studied. The structure of the halide double perovskite $Cs_2AgBiBr_6$ was relaxed, using a monomorphous and a polymorphous structure, and the energy and the band gap were calculated for each relaxed structure. The calculations corresponding to the monomorphous and the polymorphous structure showed deviations in both total energy and band gap. Comparing these deviations to the ones resulting from the same calculations of a simple perovskite, $CsPbBr_3$, they are significantly smaller. In order to obtain a deeper understanding of this phenomena, a phonon dispersion graph was produced where three imaginary modes were identified. One mode corresponded to the X-symmetry point and two triply degenerated modes were found at the Γ-symmetry point. The two modes at the Γ-point were analyzed further by studying the potential energy surfaces along the modes. Comparing these potential energy surfaces with the ones corresponding to the M- and R-modes of $CsPbBr_3$ it was concluded that the depth and width of the energy wells were much less prominent for the $Cs_2AgBiBr_6$. This was interpreted as the dynamics corresponding to the modes in question, which turned out to be octahedral tilting, being less prominent as well. Continuing the study by producing potential energy surfaces for the double perovskites $Cs_2InBiBr_6$ and $Cs_2AgGaBr_6$ as well the following things were noted. The former perovskite showed more octahedral tilting than $Cs_2AgBiBr_6$ while the latter did not show the anharmonic potential that represents octahedral tilting. Based on these results it was suggested that there is a connection between the octahedral tilting and the number of B-site ions with lone-pair electrons, since $Cs_2InBiBr_6$ has two B-site ions with lone-pair electrons, $Cs_2AgBiBr_6$ has one pair and $Cs_2AgGaBr_6$ has none. Lone-pair electrons are proven to have a tendency of distorting structures and creating instabilities which is exemplified by studying the octahedral tilting of perovskites. Also the effect of including the spin-orbit coupling in the calculations of energy and band gap of the $Cs_2AgBiBr_6$ was studied. This resulted in the relative energy of the system and the band gap increasing with approximately 0.04 meV and 1 meV respectively. Since the calculations including SOC did not change the results significantly, they should be reliable.

In future studies concerning the dynamical disorder in the structure and electronic properties of double perovskites, further corrections to the calculations of the energy should be included. The inclusion of semi-core electrons and calculations using different exchange-correlation functionals are possible ways of improving the results. The study could also be extended to examining the behaviour of the material when including defects or when observing a 2D structure.

Bibliography

[1] Hans Borén et al. *Kemiboken 1*. 2nd ed. Liber, 2018.

[2] Ji D. et al. “Regulatory tolerance and octahedral factors by using vacancy in APbI3 perovskites”. In: *Vacuum* 164 (2019), pp. 186–193.

[3] Volonakis G. et al. “Lead-free halide double perovskites via heterovalent substitution of noble metals”. In: *The journal of physical chemistry letters* 7.7 (2016), pp. 1254–1259.

[4] Yang R. et al. “Spontaneous octahedral tilting in the cubic inorganic cesium halide perovskites CsSnX3 and CsPbX3 (X= F, Cl, Br, I)”. In: *The journal of physical chemistry letters* 8.19 (2017), pp. 4720–4726.

[5] Asia Bibi et al. “Lead-free halide double perovskites: Toward stable and sustainable optoelectronic devices”. In: *Materials Today* 49 (2021), pp. 123–144.

[6] Menno Bokdam et al. “Assessing density functionals using many body theory for hybrid perovskites”. In: *Physical review letters* 119.14 (2017), p. 145501.

[7] Luisa F. Cabeza. *Advances in Thermal Energy Storage Systems*. 1st ed. Woodhead Publishing, 2015.

[8] Elizabeth Chu and D. Lawrence Tarazano. *A Brief History of Solar Panels*. URL: `https://www.smithsonianmag.com/sponsored/brief-history-solar-panels-180972006/`. (accessed: 23.05.2022).

[9] Office of Energy Efficiency and Renewable Energy. *Solar Photovoltaic Cell Basics*. URL: `https://www.energy.gov/eere/solar/solar-photovoltaic-cell-basics`. (accessed: 23.05.2022).

[10] Douglas H Fabini, Ram Seshadri, and Mercouri G Kanatzidis. “The underappreciated lone pair in halide perovskites underpins their unusual properties”. In: *MRS Bulletin* 45.6 (2020), pp. 467–477.

[11] Lingyuan Gao et al. “Metal cation s lone-pairs increase octahedral tilting instabilities in halide perovskites”. In: *Materials Advances* 2.14 (2021), pp. 4610–4616.

[12] Gonzalo Garcıa-Espejo et al. “Mechanochemical synthesis of three double perovskites: Cs 2 AgBiBr 6,(CH 3 NH 3) 2 TlBiBr 6 and Cs 2 AgSbBr 6”. In: *Nanoscale* 11.35 (2019), pp. 16650–16657.

[13] Feliciano Giustino. *Materials Modelling using Density Functional Theory*. 1st ed. Oxford University Press, 2014.

[14] Enrico Greul et al. “Highly stable, phase pure Cs 2 AgBiBr 6 double perovskite thin films for optoelectronic applications”. In: *Journal of Materials Chemistry A* 5.37 (2017), pp. 19972–19981.

[15] David J Griffiths. *Introduction to Quantum Mechanics*. 2nd ed. Pearson Education International, 2005.

[16] Philip Hofmann. *Solid state physics - An introduction.* 2nd ed. Wiley-vhc, 2015.

[17] Ping Hou et al. “Precursor engineering for high-quality Cs 2 AgBiBr 6 films toward efficient lead-free double perovskite solar cells”. In: *Journal of Materials Chemistry C* 9.30 (2021), pp. 9659–9669.

[18] Erik Jedvik Granhed. “Vibrational and Structural Characterisation in Two Perovskite Challenges: A Density Functional Theory Study”. In: (2019).

[19] Simone Meloni et al. “Valence and conduction band tuning in halide perovskites for solar cell applications”. In: *Journal of Materials Chemistry A* 4.41 (2016), pp. 15997–16002.

[20] Laura Schade et al. “Structural and optical properties of Cs2AgBiBr6 double perovskite”. In: *ACS Energy Letters* 4.1 (2018), pp. 299–305.

[21] William Shockley and Hans J Queisser. “Detailed balance limit of efficiency of p-n junction solar cells”. In: *Journal of applied physics* 32.3 (1961), pp. 510–519.

[22] Karen Steward. *Cation vs Anion: Definition, Chart and the Periodic Table.* URL: `https://www.technologynetworks.com/analysis/articles/cation-vs-anion-definition-chart-and-the-periodic-table-322863`. (accessed: 26.01.2022).

[23] Sebastian Svanström. “The life and death of perovskites: Interfacial function and degradation of lead halide perovskites studied by photoelectron spectroscopy”. In: (2021).

[24] Katarzyna Tkacz-Śmiech, A Koleżyński, and WS Ptak. “Chemical bond in ferroelectric perovskites”. In: *Ferroelectrics* 237.1 (2000), pp. 57–64.

[25] VASP. *The VASP Manual.* URL: `https://www.vasp.at/wiki/index.php/The_VASP_Manual`. (accessed: 18.05.2022).

[26] Hua Wu et al. “Mixed-Halide Double Perovskite Cs2AgBiX6 (X= Br, I) with Tunable Optical Properties via Anion Exchange”. In: *ChemSusChem* 14.20 (2021), pp. 4507–4515.

[27] Ruo Xi Yang et al. “Assessment of dynamic structural instabilities across 24 cubic inorganic halide perovskites”. In: *The Journal of chemical physics* 152.2 (2020), p. 024703.

[28] Federico Zahariev, Sarom Sok Leang, and Mark S Gordon. “Functional derivatives of meta-generalized gradient approximation (meta-GGA) type exchange-correlation density functionals”. In: *The Journal of Chemical Physics* 138.24 (2013), p. 244108.

[29] Xin-Gang Zhao et al. “Polymorphous nature of cubic halide perovskites”. In: *Physical Review B* 101.15 (2020), p. 155137.

A

Appendix

INCAR used during relaxation and final energy calculations

```
METAGGA = SCAN
NSW = 100; NSW = 0 # for relaxing/final calculations
ISMEAR = 0
SIGMA = 0.1
ENCUT = 750
EDIFF = 1e-5
NELMIN = 4
NELM = 120
ADDGRID = T
PREC = acc
ALGO = norm
LCHARG = F
LWAVE = F
LREAL = F

LMAXMIX = 4
LASPH = T

KPAR = 4
NPAR = 8
LPLANE = T
IBRION = 2; ISIF=3
```

DEPARTMENT OF PHYSICS
CHALMERS UNIVERSITY OF TECHNOLOGY
Gothenburg, Sweden
www.chalmers.se

CHALMERS
UNIVERSITY OF TECHNOLOGY